Published in final edited form as:
J Bone Miner Res. 2014 February ; 29(2): 304–315. doi:10.1002/jbmr.2038.

Delayed bone regeneration is linked to chronic inflammation in murine muscular dystrophy

Rana Abou-Khalil, PhD[a,1], **Frank Yang, BS**[b,1], **Marie Mortreux, MS**[b], **Shirley Lieu, BS**[b], **Yan-Yiu Yu, PhD**[b], **Maud Wurmser, BS**[b], **Catia Pereira, BS**[a], **Frédéric Relaix, PhD**[c], **Theodore Miclau, MD**[b], **Ralph S. Marcucio, PhD**[b], and **Céline Colnot, PhD**[a,d]

[a]INSERM U781, Université Paris Descartes-Sorbonne Paris Cité, Institut Imagine, Hôpital Necker Enfants Malades, Paris, France

[b]Department of Orthopaedic Surgery, University of California at San Francisco, San Francisco, USA

[c]INSERM, UMR-S 787, UPMC Paris VI, Institut de Myologie, Faculté de Médecine Pitié-Salpétrière, Paris, France

Abstract

Duchenne muscular dystrophy (DMD) patients exhibit skeletal muscle weakness with continuous cycles of muscle fiber degeneration/regeneration, chronic inflammation, low bone mineral density and increased risks of fracture. Fragility fractures and associated complications are considered as a consequence of the osteoporotic condition in these patients. Here, we aimed to establish the relationship between muscular dystrophy and fracture healing by assessing bone regeneration in mdx mice, a model of DMD with absence of osteoporosis. Our results illustrate that muscle defects in mdx mice impact the process of bone regeneration at various levels. In mdx fracture calluses, both cartilage and bone deposition were delayed followed by a delay in cartilage and bone remodeling. Vascularization of mdx fracture calluses was also decreased during the early stages of repair. Dystrophic muscles are known to contain elevated numbers of macrophages contributing to muscle degeneration. Accordingly, we observed increased macrophage recruitment in the mdx fracture calluses and abnormal macrophage accumulation throughout the process of bone regeneration. These changes in the inflammatory environment subsequently had an impact on the recruitment of osteoclasts and the remodeling phase of repair. Further damage to the mdx muscles, using a novel model of muscle trauma, amplified both the chronic inflammatory response and the delay in bone regeneration. In addition, PLX3397 treatment of mdx mice, a cFMS inhibitor in monocytes, partially rescued the bone repair defect through increasing cartilage deposition and decreasing macrophage number. In conclusion, chronic inflammation in mdx mice contributes to the fracture healing delay and is associated with a decrease in angiogenesis and a transient delay in osteoclast recruitment. By revealing the role of dystrophic muscle in regulating the inflammatory response during bone repair, our results emphasize the implication of muscle in

[d]Corresponding author: Céline Colnot, INSERM U781, Université Paris Descartes-Sorbonne Paris Cité, Institut Imagine, Tour Lavoisier 2ème étage, Hôpital Necker-Enfants Malades, 149 rue de Sèvres-75015 Paris, France, Tel 33 01 72 60 64 32, Fax 33 01 72 60 64 30, celine.colnot@inserm.fr.
[1]These authors contributed equally to this work.

Disclosures

All authors state that they have no conflicts of interest.

Author Contributions

CC is corresponding author and directed the study. RAK and FY are first authors. Conception and design of research: CC, RAK, FR, RM, TM; Performed research: RAK, FY, MM, SL, YYY, MW, CP; Data collection: RAK, FY, MM, SL, YYY, MW; Data analysis and interpretation: RAK, FY, FR, RM, TM, CC; Drafting Manuscript: RAK, FY, CC. All authors discussed the results and their implications and commented on the manuscript.

the normal bone repair process and may lead to improved treatment of fragility fractures in DMD patients.

Keywords

Bone; regeneration; chronic inflammation; macrophage; cartilage; muscle regeneration; muscular dystrophy; angiogenesis; osteoclastogenesis

Introduction

Many clinical and experimental observations suggest that skeletal muscle plays a role in bone regeneration. Open fractures associated with soft tissue damage and caused by severe trauma have a high incidence of non-union (1). Also, soft tissue grafting such as muscle or fasciocutaneous flaps, is known to be beneficial for the treatment of open fractures (2). Intact muscle around the bone is key to bone repair (2–4). Yet, it is not clear whether the muscle vasculature, the inflammatory cells or other muscle components support bone repair. Bone regeneration involves numerous molecular pathways and cell types that may come from various sources including muscle (5–11). The inflammatory response following injury is essential to initiate the regenerative process and can be triggered by bone tissue damage as well as damage to the vasculature and muscle. Inflammation is important for callus formation and for the subsequent phases of healing during cartilage/ bone deposition and callus remodeling (12–15). The extent of injury to bone and adjacent muscle can therefore impact the inflammatory response and the overall healing process leading to delayed consolidation. Perturbations in the normal phases of repair can also be caused by age, chronic inflammation and other pathological conditions (16).

In Duchenne muscular dystrophy (DMD) patients, who lack the dystrophin gene, fractures often occur following minimal trauma. This muscular dystrophy is characterized by chronic muscle tissue damage that is associated with numerous centrally nucleated fibers and continuous cycles of myofiber degeneration/necrosis and regeneration. This genetic disease primarily affects the assembly of muscle fibers leading to the exhaustion of the pool of muscle-resident stem cells or satellite cells. Initially, satellite cells increase in activation and efficiently regenerate the dystrophic muscle, to likely compensate for the defects (17–19). Subsequently, the pathologic environment of DMD muscles leads to chronic inflammation, fibrosis, fat infiltration and impaired vasoregulation. This pathologic environment prompts a non-permissive satellite cell-mediated regeneration, resulting in a complete loss of muscle function (17–19). DMD patients also exhibit bone defects with reduced bone mass, higher bone resorption and increased susceptibility to bone fracture (20–23). The loss of bone density is primarily due to loss of ambulation and is sharpened with the progression of the disease (23–27). Although fractures in DMD patients generally heal, it is not clear whether healing complications are mainly associated with osteoporosis or possibly related to the muscular disorder and skeletal muscle weakness. In this study, we aimed to determine the association between muscular dystrophy and bone healing independent of osteoporosis. We used the mdx mouse model of human DMD pathology. The muscle regenerative capacities of mdx mice only decline at very advanced age, but they exhibit increased inflammation and numerous centrally-nucleated fibers as early as 21 days of life. By 3 months of age, all of the muscle fibers are centro-nucleated and associated with repeated cycles of degeneration and regeneration (28–31). Like DMD patients, mdx mice show low bone mineral density and reduced mechanical resistance with osteopenia but do not exhibit osteoporosis or spontaneous fractures (20–22, 32). The reduced bone quality may be directly or indirectly related to the lack of dystrophin and muscle weakness or unknown intrinsic factors.

However, it is still unknown whether a continuously regenerative muscle could affect bone quality and bone regeneration.

To functionally address the effects of muscle degeneration on bone repair, we assessed the bone regenerative capacities of mdx mice and showed a delay in fracture healing associated with increased macrophage recruitment and, decreased angiogenesis and osteoclastogenesis. Severe damage to the muscle at the time of fracture amplified the state of chronic inflammation and further delayed bone regeneration, while inhibition of macrophages improved bone regeneration in mdx mice.

Materials and Methods

Animals

C57BL/10ScNj and mdx (C57BL/10ScSn-*Dmd*^{mdx}/J X-linked dystrophin gene) mice were obtained from Jackson Laboratory (Bar Harbor, ME). Animals were bred and all procedures were conducted according to the UCSF Institutional Animal Care and Use Committee. Three-month-old *mdx* males and age-matched wild type C57 BL/10 mice were used to conduct all experiments.

Non-stabilized fractures

Mdx and wild type males were anesthetized with an intraperitoneal injection of a 1:1 solution of 50mg/ml ketamine and 0.5mg/ml dexmedetomidine (50mg/kg body weight). A non-stabilized tibial fracture was created in the mid-diaphysis of the right tibia via three-point bending as previously described in Colnot et al. (14). Briefly, the tibia was placed on the fracture jig, and a 500g weight was dropped from 3.5 cm to create the fracture. Mice were revived with an intraperitoneal injection of 5mg/ml atipamezole (50mg/kg body weight) and were then monitored for signs of physical discomfort following a subcutaneous injection of 0.03mg/ml buprenorphine (0.05mg/kg body weight).

Non-stabilized fractures and muscle injuries

Closed fractures were induced via three-point bending as described above. Just prior to fracture, the muscles adjacent to the tibia were placed on the fracture jig, and the weight was dropped from 3.5 cm to induce 3 impacts distributed equally along the muscle. Mice were revived and monitored closely until sacrifice as described above. Longitudinal sections and hematoxylin and eosin (H&E) staining were performed to visualize centro-nucleated fibers and muscle regeneration. Transversal sections and hematoxylin and eosin (H&E) staining were also performed to assess muscle regeneration in wild type mice (n=3). Normal and centro-nucleated regenerating myofibers were quantified using ImageJ (National Institutes of Health, USA) (33).

Histological and histomorphometric analyses

Mice were sacrificed by cervical dislocation following an overdose intraperitoneal injection of 4% tribromoethanol and callus tissues were collected at days 5, 7, 14, 21 and 28 days post-fracture (n=5 or 6 per group). Samples were fixed in 4% paraformaldehyde overnight, decalcified in 19% EDTA (pH 7.4) for 14 days at 4°C and, subsequently, embedded in paraffin. Serial 10μm longitudinal sections were collected throughout the entire callus tissue using a Leica microtome (Leica Microsystems GmbH, Wetzler, Germany). To compare fracture repair rates between mdx and wild type mice, histomorphometric analyses of total callus, cartilage, and trabecular bone volumes were performed via Adobe Photoshop as previously described in Colnot et. al. (14) and Lu et. al. (34). A minimum of seven equidistant sections spaced at 300 μm apart throughout the callus was evaluated. To

visualize cartilage within each callus, every tenth section was stained with Safranin-O/Fast Green, which stains cartilage as red and all other tissues as green. To visualize trabecular bone within each callus, adjacent sections were stained with modified Milligan's Trichrome, which stains trabecular and cortical bone as blue and soft tissues as red. Images of stained sections were captured using a Leica DM 5000 B light microscope (Leica Microsystems GmbH, Wetzler, Germany) with an attached high-resolution digital c-mount camera (Diagnostic Instruments, Inc., Sterling Heights, MI). The number of pixels comprising each tissue was used to estimate area. Callus area was determined by selecting all pixels within the callus excluding cortical bone and bone marrow compartments. Cartilage area was determined by selecting all pixels stained by Safranin-O. Trabecular bone area was determined by selecting all pixels stained as blue after modified Milligan's Trichrome and then deselecting those within cortical bone. The total area of the callus, cartilage, and trabecular bone in mm2 was determined by dividing the total pixels by the numeric value of pixels/mm2, which was found using a 1mm scale bar. The total volumes of the callus, cartilage, and trabecular bone were calculated in mm3 using the equation for a conical frustum and Cavalieri's Principle: $\mathrm{Volume}=\frac{1}{3}\mathrm{h}\sum_{\mathrm{i}-1}^{\mathrm{n}-1}(\mathrm{A_i}+\mathrm{A_{i+1}}+\sqrt{\mathrm{A_iA_{i+1}}}).\mathrm{h}$ was the distance between sections and equal to 300 μm, n was the total number of sections analyzed for each callus sample, A_i and A_{i+1} were the areas of callus, cartilage, or bone in sequential sections.

PLX3397 treatment

Mdx mice were fed with PLX3397 chow (provided by Plexxikon Inc., Berkeley, CA) or control diet for 7 days prior to non-stabilized fracture and throughout the fracture healing process (n=5 or 6 per group). Samples were harvested 7 days post-fracture and processed for histomorphometric analyses as described above.

Antibodies

Affinity-purified rat anti-mouse CD31/PECAM antibody was purchased from BD Pharmingen (San Diego, CA) to detect endothelial cells. Affinity-purified rat anti-mouse F4/80 antibody was purchased from eBioscience (San Diego, CA) to detect macrophages.

Immunohistochemistry and TRAP staining

Immunohistochemistry staining was performed for each antibody on slides prepared from sections located 300μm apart throughout the callus. After deparaffinization and rehydration, sections were washed with 0.3% Triton X-100 in PBS 1X. Sections were subsequently treated with 10 μg/mL proteinase K at 37°C for retrieval of antigenicity. Endogenous peroxidase activity and non-specific binding sites were blocked by incubating the sections in 0.3% H_2O_2 in PBS 1X and 5% goat serum in PBS 1X, respectively. Sections were then incubated with diluted primary antibody in 5% goat serum (1:100) at 4°C overnight. Sections were next incubated with diluted biotinylated anti-rat secondary antibody (BD Pharmingen, San Diego, CA) in 5% goat serum (1:250). Subsequently, sections were incubated with avidin/biotin enzyme complex (Vector Laboratories, Inc., Burlingame, CA) in PBS 1X. Staining was detected using diaminobenzidine, and the tissue was counterstained with 0.1% Fast Green. On adjacent sections, tartrate resistant acid phosphatase (TRAP) staining was performed to detect osteoclasts using a leukocyte acid phosphatase kit (Sigma, St. Louis, MO).

Image analysis and stereology

PECAM+ endothelial cells, F4/80+ macrophages, and TRAP+ osteoclasts in callus tissues were quantified via stereology as previously described in (35–39). Equidistant sections

spaced at 300 μm apart were evaluated using an Olympus CAST system (Olympus, Center Valley, PA) and software by Visiopharm (Visiopharm, Hørsholm, Denmark)(n=5 or 6 per group). To compare vascular functionality between mdx and wild type mice, the outer surface area of endothelial cells within the callus was estimated by analyzing surface density (Sv). The fracture callus was outlined using low magnification (20x) to restrict sampling to the callus area. Surface density was determined under high magnification (200x) using a count frame probe that covered 50% of the area within a field of view. High-magnification fields that covered a minimum of 20% of the callus area were systematically acquired using uniform random sampling. A minimum of 200 total high-magnification fields per sample was evaluated to ensure accuracy. Randomly oriented line probes with points were then applied to each count frame probe. The line probes with points that fell onto callus tissue () and the number of intersections (i) between the outer surfaces of endothelial cells and the line probes within the count frame probes were quantified. Using this configuration, the length per line probe ($1/p_1$) was 44.41 μm, the spacing of the line probes was 131.85 μm, and the area per count frame probe was 45903.95 μm. The estimated surface density was calculated as followed: $Sv = 2 * \Sigma (i)/[(1/p_1) * \Sigma (p_1)]$.

To compare the inflammatory response and bone remodeling activity, the populations of macrophages and osteoclasts within the callus were estimated by analyzing numerical density (Nv). The fracture callus was outlined and sampling was restricted as described above. Numerical density was determined under high magnification (200x) using a count frame probe that covered 50% of the area within a field of view. High-magnification fields that covered a minimum of 20% of the callus area were systematically acquired using uniform random sampling. A minimum of 200 total high-magnification fields per sample was evaluated to ensure accuracy. Frame-associated point probes were then applied to each count frame probe. The number of point probes that fell onto callus tissue and the number of macrophages or osteoclasts within the count frame probes were quantified. Using this configuration, the area per count frame probe was 23420.38 μm and the dissector height between evaluated sections was 300 μm. The estimated numerical density was calculated as followed: $Nv = \Sigma(q)/[(a/f) * (h) * \Sigma(p_2)]$.

Real-time RT-PCR

Non-stabilized tibial fractures were created as described above. Mice were sacrificed as described above at days 7 and 14 post-fracture (n=3 per group). Following removal of surrounding skin, callus tissues and all adjacent tissues located 0.5 cm distal and proximal to the callus boundaries were collected. RNA was extracted from the tissues using Trizol reagent (Life Technologies, Carlsbad, CA), and the quantity of extracted RNA was confirmed using a NanoDrop 2000 UV-Vis Spectrophotometer (Thermo Scientific, Wilmington, DE). Commercially available primers (Table 1) were purchased from Qiagen (Germantown, MD). cDNA synthesis was performed using an iScript cDNA Synthesis Kit (Bio-Rad, Hercules, CA). Real-time PCR was performed using a QuantiTect SYBR Green PCR Kit (Qiagen, Germantown, MD) and detected using a CFX96 Touch Real-Time PCR Detection System (Bio-Rad, Hercules, CA). GAPDH was used as an internal control for all genes.

Statistical analyses

A minimum of 5 samples (3 samples for gene expression analyses) was used for each group. Statistical significance was calculated with GraphPad Prism v6.0a. Unpaired Student's t-test, One-way and Two-way ANOVA were used for statistical analyses. In all experiments, p values <0.05 were considered significant.

Results

Delayed fracture repair in a murine model of muscular dystrophy

In order to assess the effects of muscular dystrophy on bone regeneration, non-stabilized tibial fractures were induced in wild type and mdx mice. At 7 days post-fracture, histomorphometric analyses showed that cartilage and bone volumes were significantly decreased in the callus of mdx compared to wild type mice, while callus size was not affected (Fig1A–C). The proportions of cartilage and bone within the callus were also significantly decreased in mdx mice compared to wild type mice (data not shown, $p<0.01$ and $p<0.05$, respectively). At 14 days post-fracture, cartilage matrix is actively resorbed (14). In wild type mice, no significant difference in cartilage volume was detected between day 7 and day 14 of bone regeneration (Fig1A). In mdx mice, we observed a significant increase in total cartilage volume at day 14 compared to day 7 (Fig1A), indicating a delay in cartilage remodeling. ANOVA analyses throughout the entire healing process confirmed the delay in cartilage remodeling ($p<0.0001$). By day 14, bone deposition normally parallels cartilage resorption. A significant decrease in total bone volume was observed in mdx calluses compared to wild type, although callus sizes were comparable (Fig1B–C). By day 21, the cartilage was almost completely resorbed in the callus of both wild type and mdx mice (Fig1A). Day 21 is marked by active bone remodeling as shown by a significant decrease in callus and bone volume in wild type mice compared to day 14 (Fig1B–C). In mdx mice, total bone volume and callus volume were significantly increased compared to d14 (Fig1B–C). Consequently, total bone volume and total callus volume were significantly increased in mdx compared to wild type mice (Fig1B–C). ANOVA analyses confirmed these differences in osteogenesis and bone remodeling during the course of bone repair ($p<0.0001$). By day 28, total cartilage, bone and callus volumes, as well as the proportions of bone and cartilage within the callus, were comparable between mdx and wild type mice (Fig1A–C and data not shown). Moreover, callus volume was significantly decreased in mdx mice at day 28 compared to day 21 (Fig1C), indicating that remodeling eventually occurred in the callus of muscular dystrophic mice.

The delay in chondrogenesis, osteogenesis and remodeling of cartilage and bone in mdx fracture calluses were confirmed via histological and gene expression analyses. Safranin-O (SO) staining illustrated the decrease in cartilage matrix deposition in mdx compared to wild type calluses at day 7 (Fig 1D). This was accompanied by a delay in the time course of chondrogenic maturation and differentiation as well as osteogenesis at day 7 of bone regeneration. At day 7, expression of *collagen 2 (col2)*, a marker of proliferative and mature chondrocytes, and *collagen 10 (col10*) as well as *vascular endothelial growth factor* (*vegf)*, markers of hypertrophic chondrocytes, were significantly decreased within mdx callus compared to wild type callus (Fig1E and FigS1A). Expression of *collagen 1 (col1*) and *osteocalcin (oc)* were also significantly decreased in mdx callus compared to wild type by day 7 of bone regeneration (FigS1B). Subsequently, there was a delay in the resorption of cartilage matrix and in the formation of bone trabeculae in mdx calluses as shown by Milligan's Trichrome staining by d14 (Fig1F). This was confirmed by a significant decrease in *col1* and *oc* expression within mdx callus compared to wild type (Fig1G). By day 21, these bone trabeculae were remodeling and replaced by hematopoietic tissue in wild type calluses but were still present in mdx calluses (Fig1H).

Angiogenesis is impaired during bone regeneration in mdx mice

Delayed bone repair in mdx mice may be due to impaired angiogenesis, a key process for successful bone regeneration (14, 40). We assessed vascular invasion of fracture calluses using PECAM immunohistochemical staining (Fig2A). After 5 and 7 days of bone regeneration, stereological analyses of PECAM+ blood vessels revealed a significant

decrease in blood vessel surface density in mdx mice compared to wild type mice (Fig2A–B). This was paralleled with a significant decrease in *vegf* expression within mdx callus compared to wild type (FigS1A).

Osteoclastogenesis is impaired during bone regeneration in mdx mice

Bone is constantly remodeling through a balance between bone matrix synthesis by osteoblasts and bone resorption by osteoclast. An imbalanced number of osteoclasts may severely affect bone remodeling and subsequently bone regeneration (41). Mdx mice were previously reported to exhibit increased osteoclast numbers with higher osteoclast resorption parameters (20). After 5 days of bone regeneration, TRAP+ osteoclasts were quantified within the callus and stereological analyses showed a significant increase in osteoclast number in mdx mice compared to wild type mice (Fig3A–B). By day 7, however, we observed a significant decrease in TRAP+ osteoclast number as well as *mmp9* expression within mdx callus compared to wild type (Fig3A–C). After 14 days of bone regeneration, the area of new bone formation occupied by osteoclasts was reduced in mdx calluses compared to wild type, which was correlated with a significant decrease in *mmp9* expression (Fig3C–D). At day 21, delayed bone remodeling in mdx calluses was associated with an increased TRAP+ bone area compared to wild type calluses (Fig3D).

Enhanced inflammatory response during fracture repair in mdx mice

Chronic muscle tissue damage in muscular dystrophy is marked by an increase and persistent presence of macrophages (28, 29, 42). The inflammatory response to bone fracture involves monocytes/macrophages and other inflammatory cells, which are crucial to initiate bone regeneration (38, 43, 44). To determine whether delayed bone healing in mdx mice is due to an abnormal inflammatory response, we used F4/80 immunohistochemical staining to visualize and quantify macrophages at the fracture site. Comparable numbers of F4/80+ macrophages were observed within the muscle of unfractured and day 7 fractured mdx limbs, suggesting that the fracture did not increase the inflammatory state of the mdx muscle (FigS2A). Within the fracture callus, however, we observed a significant increase in the number of F4/80+ macrophages in mdx mice compared to wild type by days 5 and 7 of bone regeneration (Fig4A–B). This was paralleled with a significant increase in *cd68* expression within mdx callus compared to wild type at day 7 of bone regeneration (Fig4C). By day 14, *cd68* expression was still increased within mdx callus compared to wild type (Fig4C). F4/80+ macrophages persisted within mdx calluses at later time points of bone regeneration, whereas, in wild type fracture calluses, macrophages were progressively cleared between day 14 and day 21 post-fracture (Fig4D). It is to note that, in mdx mice, numerous F4/80+ macrophages were concentrated at the periphery of the callus and at the interface between bone and muscle (Fig4D, d14 bottom panel).

Muscle injury in muscular dystrophic mice further delays fracture healing through increasing inflammatory response

Severe muscle damage is known to impair bone healing and mdx muscles have poor healing capacities (2, 3). Beside, muscle injury is known to induce an inflammatory response including macrophages, which are essential for normal and complete muscle regeneration (45). We next induced muscle injury combined with bone fracture and assessed the impact of muscle injury and resultant inflammatory response on bone regeneration in wild type and mdx mice. To mimic traumatic injury, the muscle surrounding the fractured tibia was exposed to three impacts along its length using the fracture apparatus. At day 7, muscle regeneration was confirmed in wild type muscle with the presence of centrally-nucleated regenerating myofibers within injured muscle compared to uninjured (FigS3). At 7 days post-fracture, histomorphometric analyses showed a significant decrease in both cartilage

and callus size in wild type mice with fracture and muscle injury compared to wild type mice with fracture alone (Fig5A and Fig5C). At 14 days post fracture, no significant difference in cartilage volume was detected between the two groups. However, bone volume and callus size were significantly decreased in wild type fractures with muscle injury compared to fracture alone, indicating a delay in bone deposition after muscle injury (Fig5B–C). By day 21, cartilage was completely resorbed in wild type calluses with fracture injury alone compared to wild type fractures with muscle injury (Fig5A), indicating a significant delay in cartilage remodeling due to the muscle injury. Muscle injury also had an impact on bone regeneration in mdx mice, with a significant decrease in callus size at all stages of repair (Fig5C). By day 21, there was an increase in cartilage volume in mdx mice with muscle injury compared to mdx without muscle injury (Fig5A). Overall, muscle injury amplified the delay in the process of bone regeneration in mdx mice through delays in cartilage and bone deposition as well as cartilage and callus remodeling.

We evaluated muscle regeneration in wild type and mdx mice with bone fracture combined with muscle injury (Fig5D). After 7 days of regeneration, histology revealed centrally-nucleated fibers, indicating neo-regenerating fibers in wild type mice with fracture and muscle injury compared to wild type with fracture alone (Fig5D). In mdx mice with fracture alone, H&E staining showed centrally-nucleated fibers, which are classic signs of the pathology (Fig5D). Muscle injury further enhanced the presence of centrally-nucleated regenerating fibers in mdx mice with combined muscle and bone injuries (Fig5D).

The additional delay in bone regeneration in the presence of muscle injury was caused by amplified defects in vascularization and inflammatory response. At day 7 post-muscle and fracture injuries, stereological analyses of PECAM immunohistochemical staining showed a significant decrease in blood vessel surface density within the calluses of mdx fractures with muscle injury compared to those of wild type fractures with muscle injury and of mdx fractures without muscle injury (Fig5E). The number of F4/80+ macrophages was significantly increased in the mdx fracture with muscle injury compared to wild type fractures with muscle injury and of mdx fractures without muscle injury (Fig5F). These defects in vascularization and inflammation further impacted bone regeneration in muscular dystrophy.

Reduced macrophage recruitment and improved fracture healing in mdx mice treated with PLX3397

To confirm the role of chronic inflammation in the delay of fracture healing in mdx mice, we blocked inflammation using PLX3397, a potent inhibitor of cFMS, (46). Mdx mice were fed with PLX3397 chow for 7 days prior to fracture and until sacrifice. At day 7 post-fracture, cartilage volume, *col2* and *col10* expression were significantly increased in PLX3397- treated mdx mice compared to control mdx mice fed with a normal diet, as shown by histomorphometric and gene expression analyses (Fig6A–B). We did not observe any significant effects of PLX3397 treatment on bone and callus volumes (data not shown). Moreover, there was no significant difference in cartilage volume between PLX3397-treated mdx mice and wild type mice, suggesting that PLX3397 treatment rescued the chondrogenic delay observed in mdx mice ($p>0.05$). In parallel, we quantified F4/80+ cells and confirmed a significant decrease in macrophage number within mdx callus after PLX3397 treatment (Fig6B–C). This was confirmed by a significant decrease in *cd68* expression within mdx callus after PLX3397 treatment (Fig6D), providing strong evidence for a link between the increased inflammatory state of mdx muscle and the delay in bone healing. We did not observe any significant difference in the number of TRAP+ osteoclasts as well as *mmp9* expression between control mdx callus and PLX- treated mdx callus at day 7 of bone regeneration (Fig6E).

Discussion

In order to define the relationship between muscular dystrophy and bone healing, we explored bone regeneration in adult mdx mice, a model of Duchenne muscular dystrophy (DMD) with absence of osteoporosis. We show that the chronic and pathologic inflammatory environment of mdx mice affects bone regeneration. During the early stages of bone regeneration, mdx mice exhibit a significant delay in chondrogenesis and osteogenesis. Not only cartilage differentiation was delayed but also cartilage hypertrophy, which is essential for endochondral ossification. The osteogenic defect may result from a decrease in endochondral ossification as well as from a decrease in the osteogenic capacities of skeletal precursors (20, 47). The delay in cartilage and bone formation may also be linked to the decrease of blood vessel invasion that we have identified. Despite the normal blood vessel development in mdx mice, dystrophin deficiency in vascular smooth muscle cells has been reported to cause impaired vasoregulation (48, 49). Interestingly, blood vessel walls have recently been proposed as a source of skeletal progenitors for bone repair (50). The angiogenesis defect in mdx calluses may thus affect the recruitment of osteoblast and chondrocyte precursors at the fracture site.

DMD and mdx muscles exhibit chronic inflammation with an increased and persistent presence of macrophages, which are not found in normal healthy steady state muscle (28, 29, 42, 51, 52). Acute and chronic inflammatory responses are detrimental to normal bone repair (12, 53). Following tibial fracture, we observed an increased recruitment of macrophages in the callus of mdx mice. Macrophages have been associated with positive effects on bone repair (39, 54), but in this chronic inflammatory environment, abnormal recruitment of macrophages may impair the initial phase of bone regeneration. This chronic inflammatory environment may perturb the balance between proliferation and differentiation of skeletal stem cells as well as chondrocyte and osteoblast differentiation during bone regeneration (38, 55). Indeed, mdx mice display increased serum levels of IL6, which has been shown to inhibit the proliferation of mesenchymal stem cells (20, 56). To support the link between abnormal inflammation and delayed bone repair, we showed that severe muscle injury increases macrophage infiltration and further delays callus formation. Conversely, macrophage inhibition with PLX3397 partially rescued the fracture healing delay in mdx mice by increasing cartilage deposition, which supports endochondral ossification at later stages of repair. PLX3397 treatment specifically inhibited macrophages within mdx callus and did not affect the number of osteoclasts within mdx callus, emphasizing the role of macrophages in the mdx fracture healing phenotype.

Adding to the defects of the initial phase of bone regeneration, the pathologic and persistent inflammatory environment in mdx mice also affected cartilage, bone and callus remodeling. The remodeling phase of repair was marked with the continuous presence of F4/80+ macrophages within mdx calluses. Macrophages and osteoclasts are derived from a common hematopoietic lineage, which may tie the increased inflammation and increased osteoclastogenesis at the early stages of repair (20, 57). Following this initial phase, however, we observed a decrease in osteoclast numbers in mdx calluses, which may be due to the delay in bone deposition. Subsequently, callus remodeling was delayed although no significant differences were detected by day 28, possibly due to increased osteoclast activity and IL6 levels to compensate for the delay in osteoclast recruitment (20). Hence, the transient delay in callus remodeling reflects the delay in the entire healing process. Chronic inflammatory infiltration in dystrophic muscles is usually associated with the replacement of degenerating muscle by adipose and fibrotic tissue. In mdx mice, fibrosis is developed with aging (18 months) (51, 52, 58). Here, we did not detect any potential increase in fibrosis at the fracture site that may be linked to the healing defect (data not shown).

Altogether, our results show that the abnormal and chronic inflammatory environment at the site of bone injury in mdx mice is responsible for the delay in bone regeneration. The overall healing delay is a consequence of the initial delay in chondrogenesis and soft callus remodeling mainly due to the abnormal angiogenic and inflammatory milieu. Thus, bone regeneration is negatively affected in a pathologic and inflammatory muscle environment, revealing the role of healthy normal muscle during bone regeneration. Little is known about the interactions between muscle and bone in regulating skeletal repair. These results have relevance to Duchenne muscular dystrophy patients, who often sustain fractures following minimal trauma. In these patients, post-fracture complications are devastating and often lead to permanent loss of function (24). The aberrant inflammatory environment of dystrophic muscle delays both muscle and bone repair. Glucocorticoids and non-steroidal anti-inflammatory (NSAID) drugs are currently used to treat DMD patients (59–61). NSAID are known to be potent inhibitors of inflammatory cells and administration of NSAID can impair fracture healing in animals (62). However, the controlled inhibition of inflammation may be crucial to stimulate bone repair in pathological conditions such as muscular dystrophy.

Supplementary Material

Refer to Web version on PubMed Central for supplementary material.

Acknowledgments

This work was funded by NIH-NIAMS R01 AR057344 to CC and TM, University of California San Francisco Academic Senate, INSERM ATIP-AVENIR, Sanofi and FP7 Marie Curie IRG to CC. PLX3397 was provided by Plexxikon Inc.

References

1. Sudkamp NP, Haas NP, Sinnig M, Sottmann G, Tscherne H. [Incidence of pseudarthroses in open fractures: analysis of 948 open fractures]. Aktuelle Traumatol. 1993; 23(2):59–67. PubMed PMID: 8098572. [PubMed: 8098572]
2. Yazar S, Lin CH, Lin YT, Ulusal AE, Wei FC. Outcome comparison between free muscle and free fasciocutaneous flaps for reconstruction of distal third and ankle traumatic open tibial fractures. Plastic and reconstructive surgery. 2006; 117(7):2468–2475. discussion 76-7.PubMed PMID: 16772958. [PubMed: 16772958]
3. Evans KD, Oberbauer AM. Alendronate inhibits VEGF expression in growth plate chondrocytes by acting on the mevalonate pathway. Open Orthop J. 2009; 3:83–88. Epub 2009/10/17.PubMed PMID: 19834579; PubMed Central PMCID: PMC2761671. [PubMed: 19834579]
4. Cairns DM, Uchimura T, Kwon H, Lee PG, Seufert CR, Matzkin E, et al. Muscle cells enhance resistance to pro-inflammatory cytokine-induced cartilage destruction. Biochem Biophys Res Commun. 2010; 392(1):22–28. Epub 2010/01/02. PubMed PMID: 20043873; PubMed Central PMCID: PMC2841304. [PubMed: 20043873]
5. Einhorn TA. The cell and molecular biology of fracture healing. Clinical Orthopaedics and Related Research. 1998; 46(355 Suppl):S7–S21. [PubMed: 9917622]
6. Ai-Aql ZS, Alagl AS, Graves DT, Gerstenfeld LC, Einhorn TA. Molecular mechanisms controlling bone formation during fracture healing and distraction osteogenesis. J Dent Res. 2008; 87(2):107–118. Epub 2008/01/26. PubMed PMID: 18218835; PubMed Central PMCID: PMC3109437. [PubMed: 18218835]
7. Einhorn TA, Majeska RJ, Rush EB, Levine PM, Horowitz MC. The expression of cytokine activity by fracture callus. J Bone Miner Res. 1995; 10(8):1272–1281. [PubMed: 8585432]
8. Phillips AM. Overview of the fracture healing cascade. Injury. 2005; 36(Suppl 3):S5–S7. Epub 2005/09/29. PubMed PMID: 16188551. [PubMed: 16188551]

9. Tsiridis E, Upadhyay N, Giannoudis P. Molecular aspects of fracture healing: which are the important molecules? Injury. 2007; 38 Suppl 1:S11–S25. Epub 2007/03/27. PubMed PMID: 17383481. [PubMed: 17383481]
10. Dimitriou R, Tsiridis E, Giannoudis PV. Current concepts of molecular aspects of bone healing. Injury. 2005; 36(12):1392–1404. Epub 2005/08/17. PubMed PMID: 16102764. [PubMed: 16102764]
11. Hamrick MW, McNeil PL, Patterson SL. Role of muscle-derived growth factors in bone formation. J Musculoskelet Neuronal Interact. 2010; 10(1):64–70. Epub 2010/03/02. PubMed PMID: 20190381. [PubMed: 20190381]
12. Gerstenfeld LC, Cho TJ, Kon T, Aizawa T, Tsay A, Fitch J, et al. Impaired fracture healing in the absence of TNF-alpha signaling: the role of TNF-alpha in endochondral cartilage resorption. J Bone Miner Res. 2003; 18(9):1584–1592. PubMed PMID: 12968667. [PubMed: 12968667]
13. Thompson Z, Miclau T, Hu D, Helms JA. A model for intramembranous ossification during fracture healing. J Orthop Res. 2002; 20(5):1091–1098. PubMed PMID: 12382977. [PubMed: 12382977]
14. Colnot C, Thompson Z, Miclau T, Werb Z, Helms JA. Altered fracture repair in the absence of MMP9. Development. 2003; 130(17):4123–4133. PubMed PMID: 12874132. [PubMed: 12874132]
15. Palomares KT, Gleason RE, Mason ZD, Cullinane DM, Einhorn TA, Gerstenfeld LC, et al. Mechanical stimulation alters tissue differentiation and molecular expression during bone healing. J Orthop Res. 2009; 27(9):1123–1132. Epub 2009/02/27. PubMed PMID: 19242967; PubMed Central PMCID: PMC2726267. [PubMed: 19242967]
16. Lynch JR, Taitsman LA, Barei DP, Nork SE. Femoral nonunion: risk factors and treatment options. J Am Acad Orthop Surg. 2008; 16(2):88–97. Epub 2008/02/07. PubMed PMID: 18252839. [PubMed: 18252839]
17. Morgan JE, Zammit PS. Direct effects of the pathogenic mutation on satellite cell function in muscular dystrophy. Experimental cell research. 2010; 316(18):3100–3108. Epub 2010/06/16.PubMed PMID: 20546725. [PubMed: 20546725]
18. Reimann J, Irintchev A, Wernig A. Regenerative capacity and the number of satellite cells in soleus muscles of normal and mdx mice. Neuromuscular disorders : NMD. 2000; 10(4–5):276–282. PubMed PMID: 10838255. [PubMed: 10838255]
19. Partridge T. Pathophysiology of muscular dystrophy. British journal of hospital medicine. 1993; 49(1):26–36. Epub 1993/01/06. PubMed PMID: 8431724. [PubMed: 8431724]
20. Rufo A, Del Fattore A, Capulli M, Carvello F, De Pasquale L, Ferrari S, et al. Mechanisms inducing low bone density in Duchenne muscular dystrophy in mice and humans. J Bone Miner Res. 2011; 26(8):1891–1903. Epub 2011/04/22. PubMed PMID: 21509823; PubMed Central PMCID: PMC3150693. [PubMed: 21509823]
21. Nakagaki WR, Bertran CA, Matsumura CY, Santo-Neto H, Camilli JA. Mechanical, biochemical and morphometric alterations in the femur of mdx mice. Bone. 2011; 48(2):372–379. Epub 2010/09/21.PubMed PMID: 20850579. [PubMed: 20850579]
22. Novotny SA, Warren GL, Lin AS, Guldberg RE, Baltgalvis KA, Lowe DA. Bone is functionally impaired in dystrophic mice but less so than skeletal muscle. Neuromuscular disorders : NMD. 2011; 21(3):183–193. Epub 2011/01/25. PubMed PMID: 21256750; PubMed Central PMCID: PMC3046261. [PubMed: 21256750]
23. Philippe V, Pruna L, Abdel Fattah M, Pascal V, Kaminsky P. Decreased bone mineral density in adult patients with muscular dystrophy. Joint, bone, spine : revue du rhumatisme. 2011; 78(6): 651–652. Epub 2011/07/06. PubMed PMID: 21727019.
24. McDonald DG, Kinali M, Gallagher AC, Mercuri E, Muntoni F, Roper H, et al. Fracture prevalence in Duchenne muscular dystrophy. Dev Med Child Neurol. 2002; 44(10):695–698. Epub 2002/11/07. PubMed PMID: 12418795. [PubMed: 12418795]
25. Bianchi ML, Morandi L, Andreucci E, Vai S, Frasunkiewicz J, Cottafava R. Low bone density and bone metabolism alterations in Duchenne muscular dystrophy: response to calcium and vitamin D treatment. Osteoporos Int. 2011; 22(2):529–539. Epub 2010/05/12. PubMed PMID: 20458570. [PubMed: 20458570]

26. Bianchi ML, Mazzanti A, Galbiati E, Saraifoger S, Dubini A, Cornelio F, et al. Bone mineral density and bone metabolism in Duchenne muscular dystrophy. Osteoporos Int. 2003; 14(9):761–767. Epub 2003/08/05. PubMed PMID: 12897980. [PubMed: 12897980]
27. Larson CM, Henderson RC. Bone mineral density and fractures in boys with Duchenne muscular dystrophy. J Pediatr Orthop. 2000; 20(1):71–74. PubMed PMID: 10641693. [PubMed: 10641693]
28. Tanabe Y, Esaki K, Nomura T. Skeletal muscle pathology in X chromosome-linked muscular dystrophy (mdx) mouse. Acta Neuropathol. 1986; 69(1–2):91–95. Epub 1986/01/01. PubMed PMID: 3962599. [PubMed: 3962599]
29. Porter JD, Khanna S, Kaminski HJ, Rao JS, Merriam AP, Richmonds CR, et al. A chronic inflammatory response dominates the skeletal muscle molecular signature in dystrophin-deficient mdx mice. Hum Mol Genet. 2002; 11(3):263–272. Epub 2002/02/02. PubMed PMID: 11823445. [PubMed: 11823445]
30. Cullen MJ, Jaros E. Ultrastructure of the skeletal muscle in the X chromosome-linked dystrophic (mdx) mouse. Comparison with Duchenne muscular dystrophy. Acta Neuropathol. 1988; 77(1): 69–81. Epub 1988/01/01. PubMed PMID: 3239377. [PubMed: 3239377]
31. Partridge T. Animal models of muscular dystrophy--what can they teach us? Neuropathology and applied neurobiology. 1991; 17(5):353–363. Epub 1991/10/01. PubMed PMID: 1758568. [PubMed: 1758568]
32. Sicinski P, Geng Y, Ryder-Cook AS, Barnard EA, Darlison MG, Barnard PJ. The molecular basis of muscular dystrophy in the mdx mouse: a point mutation. Science. 1989; 244(4912):1578–1580. PubMed PMID: 2662404. [PubMed: 2662404]
33. Abou-Khalil R, Le Grand F, Pallafacchina G, Valable S, Authier FJ, Rudnicki MA, et al. Autocrine and paracrine angiopoietin 1/Tie-2 signaling promotes muscle satellite cell self-renewal. Cell Stem Cell. 2009; 5(3):298–309. Epub 2009/09/08.[pii] 10.1016/j.stem.2009.06.001. PubMed PMID: 19733541. [PubMed: 19733541]
34. Lu C, Miclau T, Hu D, Hansen E, Tsui K, Puttlitz C, et al. Cellular basis for age-related changes in fracture repair. J Orthop Res. 2005; 23(6):1300–1307. Epub 2005/06/07. PubMed PMID: 15936915; PubMed Central PMCID: PMC2844440. [PubMed: 15936915]
35. Lu C, Hansen E, Sapozhnikova A, Hu D, Miclau T, Marcucio RS. Effect of age on vascularization during fracture repair. J Orthop Res. 2008; 26(10):1384–1389. Epub 2008/05/09. PubMed PMID: 18464248; PubMed Central PMCID: PMC2846969. [PubMed: 18464248]
36. Lu C, Saless N, Hu D, Wang X, Xing Z, Hou H, et al. Mechanical stability affects angiogenesis during early fracture healing. J Orthop Trauma. 2011; 25(8):494–499. Epub 2011/07/09. PubMed PMID: 21738063; PubMed Central PMCID: PMC3167470. [PubMed: 21738063]
37. Lu C, Xing Z, Wang X, Mao J, Marcucio RS, Miclau T. Anti-inflammatory treatment increases angiogenesis during early fracture healing. Arch Orthop Trauma Surg. 2012; 132(8):1205–1213. Epub 2012/05/25. PubMed PMID: 22622792. [PubMed: 22622792]
38. Wang X, Yu YY, Lieu S, Yang F, Lang J, Lu C, et al. MMP9 regulates the cellular response to inflammation after skeletal injury. Bone. 2013; 52(1):111–119. Epub 2012/09/27. PubMed PMID: 23010105; PubMed Central PMCID: PMC3513654. [PubMed: 23010105]
39. Xing Z, Lu C, Hu D, Yu YY, Wang X, Colnot C, et al. Multiple roles for CCR2 during fracture healing. Dis Model Mech. 2010; 3(7–8):451–458. Epub 2010/04/01. [pii] 10.1242/dmm.003186. PubMed PMID: 20354109. [PubMed: 20354109]
40. Maes C, Coenegrachts L, Stockmans I, Daci E, Luttun A, Petryk A, et al. Placental growth factor mediates mesenchymal cell development, cartilage turnover, and bone remodeling during fracture repair. J Clin Invest. 2006; 116(5):1230–1242. PubMed PMID: 16614757. [PubMed: 16614757]
41. Boyle WJ, Simonet WS, Lacey DL. Osteoclast differentiation and activation. Nature. 2003; 423(6937):337–342. PubMed PMID: 12748652. [PubMed: 12748652]
42. Coulton GR, Morgan JE, Partridge TA, Sloper JC. The mdx mouse skeletal muscle myopathy: I. A histological, morphometric and biochemical investigation. Neuropathology and applied neurobiology. 1988; 14(1):53–70. Epub 1988/01/01. PubMed PMID: 2967442. [PubMed: 2967442]

43. Nam D, Mau E, Wang Y, Silkstone D, Wright D, Whestone H, et al. T-lymphocytes enable osteoblast maturation during early phases of fracture repair. Orthopaedic Research Society. 2012 http://www.ors.org/abstracts/:paper#0348.
44. Claes L, Recknagel S, Ignatius A. Fracture healing under healthy and inflammatory conditions. Nat Rev Rheumatol. 2012; 8(3):133–143. Epub 2012/02/02. nrrheum.2012.1 [pii]. PubMed PMID: 22293759. [PubMed: 22293759]
45. Chazaud B, Brigitte M, Yacoub-Youssef H, Arnold L, Gherardi R, Sonnet C, et al. Dual and beneficial roles of macrophages during skeletal muscle regeneration. Exercise and sport sciences reviews. 2009; 37(1):18–22. Epub 2008/12/23. PubMed PMID: 19098520. [PubMed: 19098520]
46. Prada CE, Jousma E, Rizvi TA, Wu J, Dunn RS, Mayes DA, et al. Neurofibroma-associated macrophages play roles in tumor growth and response to pharmacological inhibition. Acta Neuropathol. 2012 sEpub 2012/10/27. PubMed PMID: 23099891.
47. Leng Y, Zheng Z, Zhou C, Zhang C, Shi X, Zhang W. A comparative study of bone marrow mesenchymal stem cell functionality in C57BL and mdx mice. Neuroscience letters. 2012; 523(2): 139–144. Epub 2012/07/07. PubMed PMID: 22766138. [PubMed: 22766138]
48. Straino S, Germani A, Di Carlo A, Porcelli D, De Mori R, Mangoni A, et al. Enhanced arteriogenesis and wound repair in dystrophin-deficient mdx mice. Circulation. 2004; 110(21): 3341–3348. PubMed PMID: 15545520. [PubMed: 15545520]
49. Ito K, Kimura S, Ozasa S, Matsukura M, Ikezawa M, Yoshioka K, et al. Smooth muscle-specific dystrophin expression improves aberrant vasoregulation in mdx mice. Hum Mol Genet. 2006; 15(14):2266–2275. PubMed PMID: 16777842. [PubMed: 16777842]
50. Grcevic D, Pejda S, Matthews BG, Repic D, Wang L, Li H, et al. In vivo fate mapping identifies mesenchymal progenitor cells. Stem Cells. 2012; 30(2):187–196. Epub 2011/11/16. PubMed PMID: 22083974. [PubMed: 22083974]
51. Acharyya S, Villalta SA, Bakkar N, Bupha-Intr T, Janssen PM, Carathers M, et al. Interplay of IKK/NF-kappaB signaling in macrophages and myofibers promotes muscle degeneration in Duchenne muscular dystrophy. J Clin Invest. 2007; 117(4):889–901. Epub Mar 22. PubMed PMID: 17380205. [PubMed: 17380205]
52. Villalta SA, Nguyen HX, Deng B, Gotoh T, Tidball JG. Shifts in macrophage phenotypes and macrophage competition for arginine metabolism affect the severity of muscle pathology in muscular dystrophy. Hum Mol Genet. 2009; 18(3):482–496. Epub 2008/11/11. PubMed PMID: 18996917; PubMed Central PMCID: PMC2638796. [PubMed: 18996917]
53. Hamrick MW, Della Fera MA, Choi YH, Hartzell D, Pennington C, Baile CA. Injections of leptin into rat ventromedial hypothalamus increase adipocyte apoptosis in peripheral fat and in bone marrow. Cell Tissue Res. 2007; 327(1):133–141. Epub 2006/10/07. PubMed PMID: 17024416. [PubMed: 17024416]
54. Alexander KA, Chang MK, Maylin ER, Kohler T, Muller R, Wu AC, et al. Osteal macrophages promote in vivo intramembranous bone healing in a mouse tibial injury model. J Bone Miner Res. 2011; 26(7):1517–1532. Epub 2011/02/10. PubMed PMID: 21305607. [PubMed: 21305607]
55. Claes L, Ignatius A, Lechner R, Gebhard F, Kraus M, Baumgartel S, et al. The effect of both a thoracic trauma and a soft-tissue trauma on fracture healing in a rat model. Acta Orthop. 2011; 82(2):223–227. Epub 2011/04/06. PubMed PMID: 21463222; PubMed Central PMCID: PMC3235295. [PubMed: 21463222]
56. Cho TJ, Kim JA, Chung CY, Yoo WJ, Gerstenfeld LC, Einhorn TA, et al. Expression and role of interleukin-6 in distraction osteogenesis. Calcif Tissue Int. 2007; 80(3):192–200. Epub 2007/03/07. PubMed PMID: 17340223. [PubMed: 17340223]
57. Wada T, Nakashima T, Hiroshi N, Penninger JM. RANKL-RANK signaling in osteoclastogenesis and bone disease. Trends in molecular medicine. 2006; 12(1):17–25. Epub 2005/12/17. PubMed PMID: 16356770. [PubMed: 16356770]
58. Serrano AL, Mann CJ, Vidal B, Ardite E, Perdiguero E, Munoz-Canoves P. Cellular and molecular mechanisms regulating fibrosis in skeletal muscle repair and disease. Current topics in developmental biology. 2011; 96:167–201. Epub 2011/05/31. PubMed PMID: 21621071. [PubMed: 21621071]

59. Fenichel GM, Florence JM, Pestronk A, Mendell JR, Moxley RT, Griggs RC 3rd, et al. Long-term benefit from prednisone therapy in Duchenne muscular dystrophy. Neurology. 1991; 41(12):1874–1877. Epub 1991/12/01. PubMed PMID: 1745340. [PubMed: 1745340]

60. De Larichaudy J, Zufferli A, Serra F, Isidori AM, Naro F, Dessalle K, et al. TNF-alpha- and tumor-induced skeletal muscle atrophy involves sphingolipid metabolism. Skeletal muscle. 2012; 2(1) Epub 2012/01/20.PubMed PMID: 22257771; PubMed Central PMCID: PMC3344678.

61. D'Angelo MG, Gandossini S, Martinelli Boneschi F, Sciorati C, Bonato S, Brighina E, et al. Nitric oxide donor and non steroidal anti inflammatory drugs as a therapy for muscular dystrophies: evidence from a safety study with pilot efficacy measures in adult dystrophic patients. Pharmacological research : the official journal of the Italian Pharmacological Society. 2012; 65(4): 472–479. Epub 2012/02/07. PubMed PMID: 22306844. [PubMed: 22306844]

62. Abdul-Hadi O, Parvizi J, Austin MS, Viscusi E, Einhorn T. Nonsteroidal anti-inflammatory drugs in orthopaedics. J Bone Joint Surg Am. 2009; 91(8):2020–2027. Epub 2009/08/05. PubMed PMID: 19651965. [PubMed: 19651965]

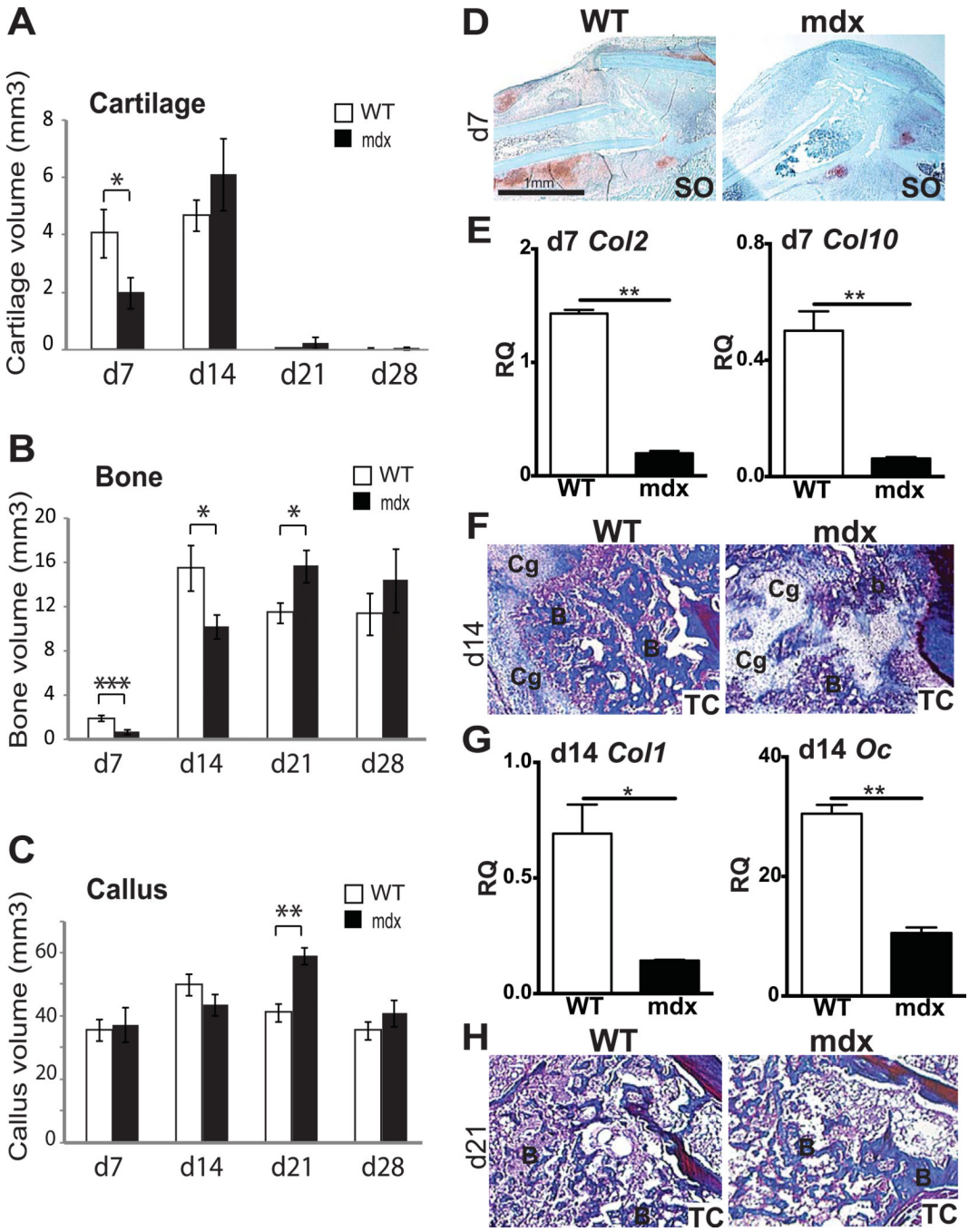

Figure 1. Effects of muscular dystrophy on tibial fracture repair in mice

Histomorphometric measurements of (A) total cartilage volume, (B) total bone volume and (C) total callus volume at days 7 (d7), 14 (d14), 21 (d21) and 28 (d28) post-fracture in wild type (WT) and mdx mice. (D) Safranin-O (SO) staining of longitudinal sections of WT (left) and mdx (right) callus tissues at day 7 (d7) of bone regeneration illustrate the proteoglycan-containing cartilage (red, D). (E) Relative quantification (RQ) by RTqPCR of *collagen 2 (col2)* (left) and *collagen 10 (col10)* (right) mRNA within wild type (WT) and mdx calluses at day 7 (d7). Expression level was normalized to GAPDH mRNA. (F–H) Trichrome (TC) staining of longitudinal sections of WT (left) and mdx (right) callus tissues at (F) day 14

(d14) and (H) day 21 (d21) of bone regeneration denote bone matrix deposition (Blue, F–H). B, bone; Cg, cartilage. (G) Relative quantification (RQ) by RTqPCR of the osteogenic markers *collagen 1 (col1)* (left) and *osteocalcin (oc)* (right) mRNA within wild type (WT) and mdx calluses at day 14 (d14). Expression level was normalized to GAPDH mRNA. Error bars represent ±SEM. One-way, two-way ANOVA and unpaired Student's t test, P values *$p<0.05$, **$p<0.001$, ***$p<0.0005$ (n=5 or 6 per group for histomorphometric analyses; n=3 for gene expression). Scale bar: 1 mm (D), 50 λm (E), 50 λm (F–G).

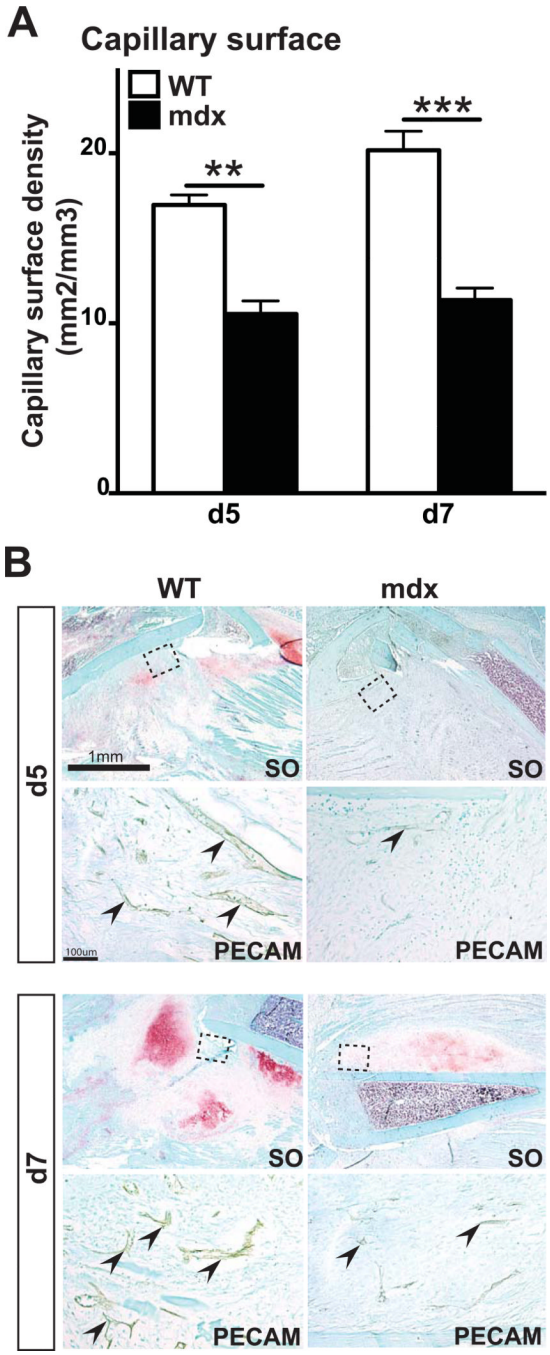

Figure 2. Effects of muscular dystrophy on vascularization of the fracture callus

(A) Stereological quantification of blood vessels within the callus of wild type (WT) and mdx mice. Blood vessel surface density is significantly decreased in mdx compared to WT mice after 5 (d5) and 7 days (d7) of bone regeneration. (B) Safranin-O (SO) staining and PECAM immunohistochemical staining (arrows, area corresponds to dashed box in SO staining) on adjacent sections of WT and mdx fracture calluses after 5 days (d5) and 7 days (d7) of bone regeneration. Error bars represent ±SEM. Unpaired student's t test, P values **p<0.001, ***p<0.0005 (n=5 or 6 per group). Scale bar: 1mm, 100 μ (B).

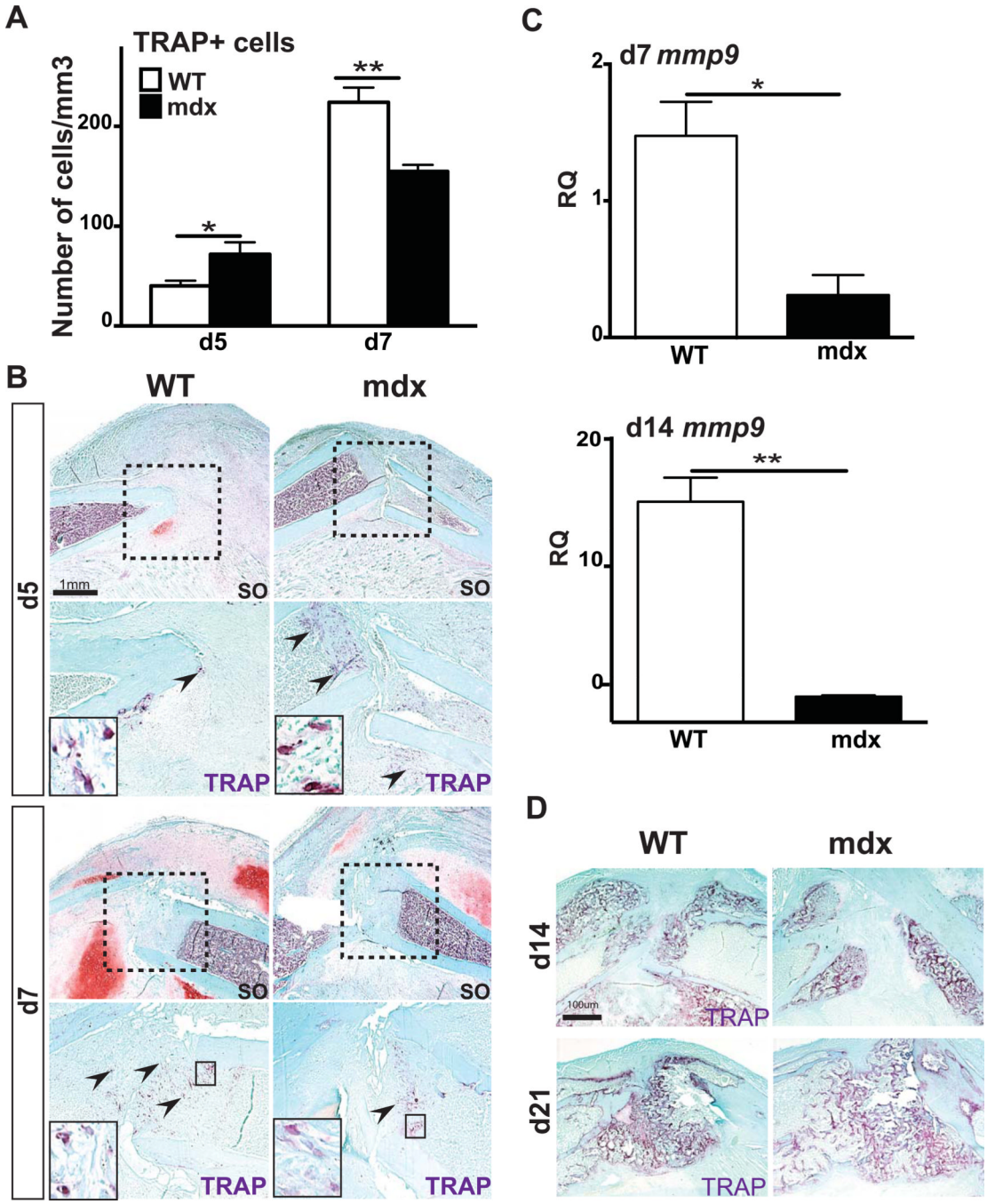

Figure 3. Effects of muscular dystrophy on osteoclasts during fracture repair

(A) Stereological quantification of TRAP+ osteoclasts within wild type (WT) and mdx calluses after 5 days (d5) and 7 days (d7) of bone regeneration. (B) Safranin-O (SO) staining and representative TRAP staining (arrows, area corresponds to dashed box in SO staining) on adjacent sections of WT and mdx fracture calluses at day 5 (d5) and day 7 (d7) of bone regeneration. (C) Relative quantification (RQ) by RTqPCR of *matrix metalloproteinase-9 (mmp9)* (right) mRNA, marker of osteoclasts, within WT and mdx calluses at day 7 (d7) and day 14 (d14). Expression level was normalized to GAPDH mRNA. (D) Representative TRAP staining in WT and mdx fracture calluses at day 14 (d14) and day 21 (d21) of bone regeneration. Error bars represent ±SEM. Student's t test, P values *p<0.05, **p<0.001 (n=5

or 6 per group for TRAP staining, n=3 per group for gene expression). Scale bar: 1mm, 100 μ (B).

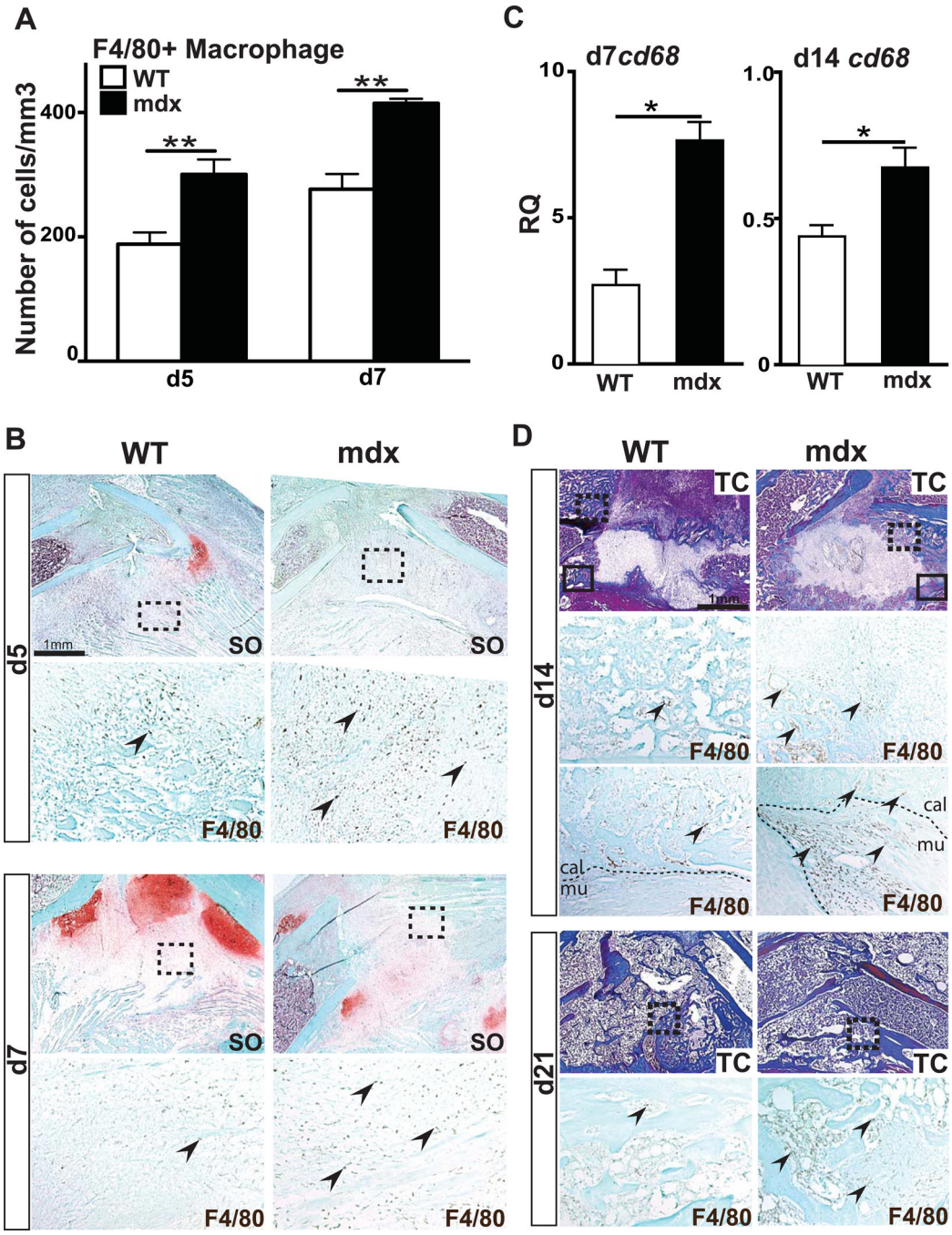

Figure 4. Effects of muscular dystrophy on macrophage recruitment during fracture repair

(A) Stereological quantification of F4/80+ cells within wild type (WT) and mdx calluses after 5 (d5) and 7 days (d7) of bone regeneration. (B) Safranin-O (SO) staining and representative F4/80 staining (arrows, area corresponds to dashed box in SO) on adjacent sections of WT and mdx calluses at day 5 (d5) and day 7 (d7) of bone regeneration. (C) Relative quantification (RQ) by RTqPCR of *cd68* mRNA, marker of macrophages, at days 7 (d7) and 14 (d14) within WT and mdx calluses. Expression level was normalized to GAPDH mRNA. (D) Trichrome (TC) staining and representative F4/80 staining (arrows, area corresponds to dashed box in TC staining) on adjacent sections of WT and mdx fracture

calluses at day 14 (d14) and day 28 (d28) of bone regeneration. By d14, there is an increase in F4/80+ macrophages at the interface between callus (cal) and muscle (mu) (arrows, area corresponds to black box in TC staining). Error bars represent ±SEM. Unpaired student's t test, P values *$p<0.05$, **$p<0.001$ (n=5 or 6 per group for F4/80 immunohistochemical staining, n=3 per group for gene expression). Scale bar: 1 mm, 100 μ (B).

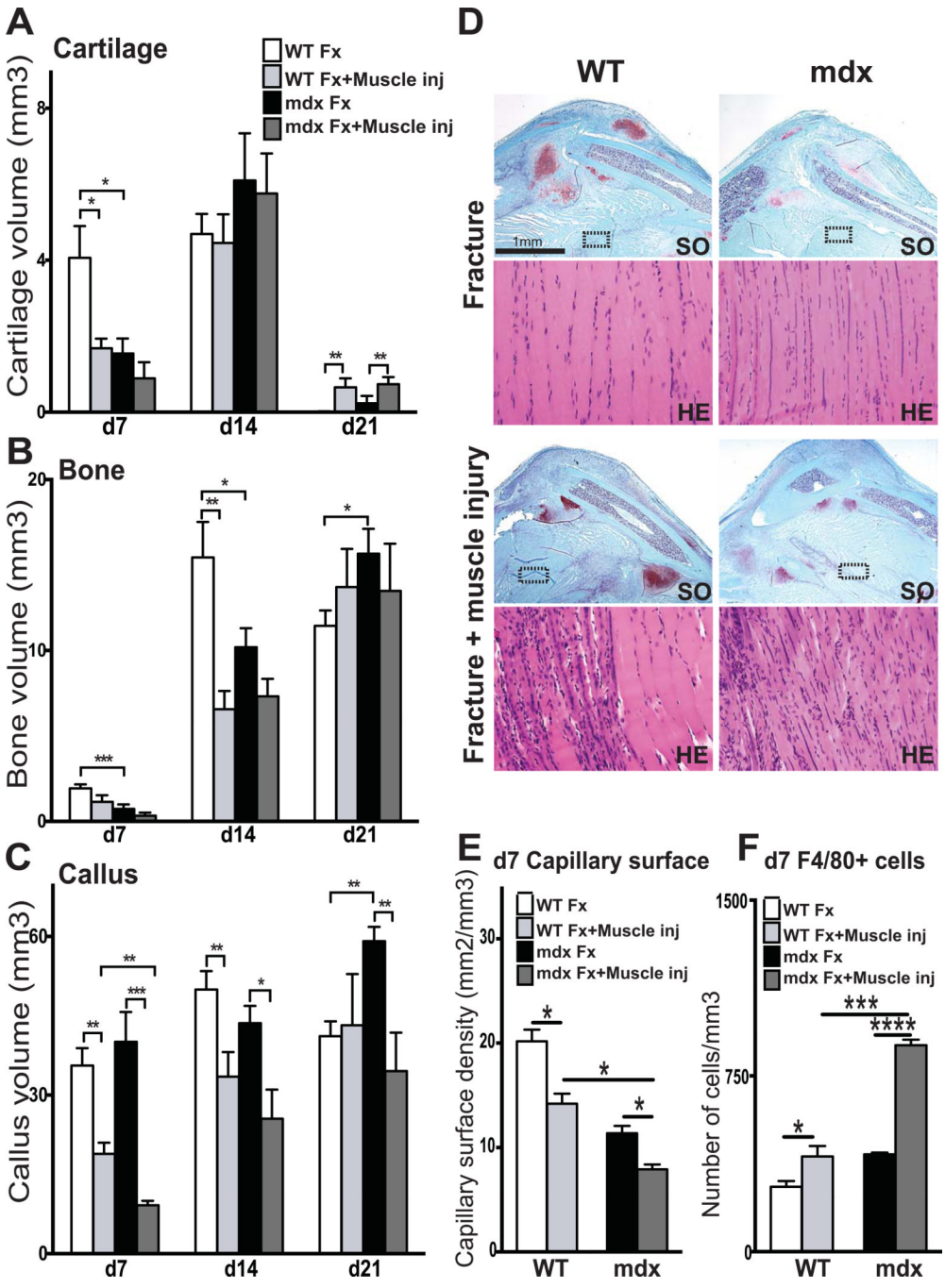

Figure 5. Combined effects of muscular dystrophy and muscle injury on fracture repair

Histomorphometric measurements of (A) total cartilage volume, (B) total bone volume and (C) total callus volume at 7 (d7), 14 (d14), 21 (d21) and 28 (d28) days post-injury in wild type (WT) and mdx mice (Fx= Bone Fracture alone; Fx+Muscle inj= Fracture combined with muscle injury). (D) Safranin-O (SO) and Hematoxylin-Eosin (H&E) staining of wild type (WT) and mdx fracture calluses after fracture alone (top) or fracture combined with muscle injury (bottom) at day 7 (d7) post-injury. (E–F) Stereological quantification of blood vessels (E) and F4/80+ macrophages (F) within WT and mdx calluses at day 7 (d7) post fracture (Fx= Bone Fracture alone; Fx+Muscle inj= Fracture combined with muscle injury). Error bars represent ±SEM. ANOVA and unpaired Student's t test, P values *p<0.05,

**p<0.001, ***p<0.0005, ****p<0.0001 (n=5 or 6 per group, n=3 per group for gene expression). Scale bar: 1 mm, 100 μ (D).

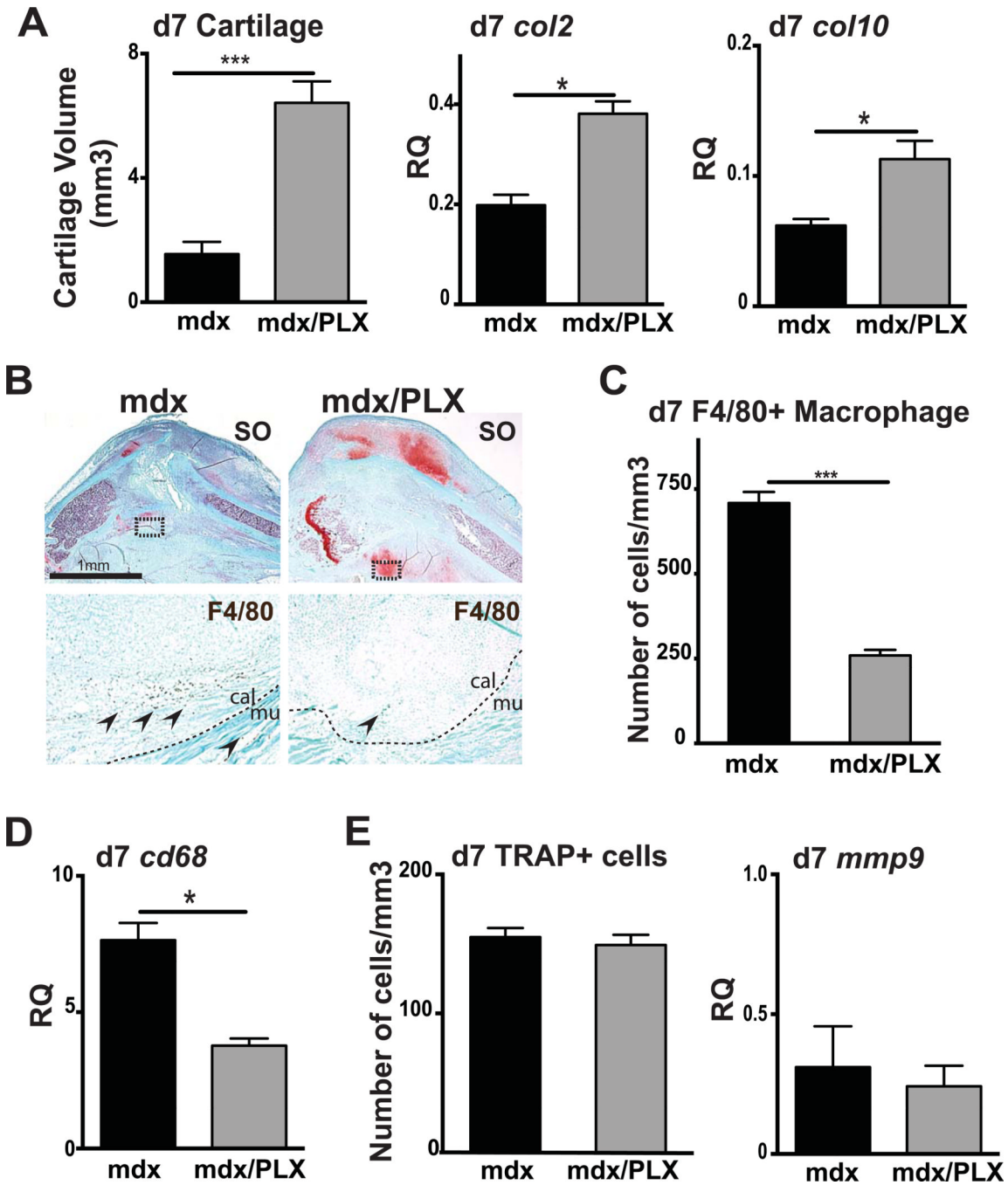

Figure 6. Effects of PLX3397 treatment, a cFMs inhibitor, on fracture healing

(A) Histomorphometric measurements of total cartilage volume at 7 days (d7) post-injury in mdx mice (mdx) and PLX3397-treated mdx mice (mdx/PLX) (left). Relative quantification (RQ) by RTqPCR of *collagen 2 (col2)* (center) and *collagen 10 (col10)* (right) mRNA within mdx and PLX3397-treated mdx calluses at day 7 (d7) post-fracture. Expression level was normalized to GAPDH mRNA. (B) Safranin-O (SO) staining and representative F4/80 staining (arrows, area corresponds to dashed box in SO staining) on adjacent sections of control mdx and PLX3397-treated mdx fracture callus (mdx/PLX) at day 7 (d7) post-injury. (C) Stereological quantification of F4/80+ cells within mdx and PLX3397-treated mdx calluses (mdx/PLX) after 7 days (d7) of bone regeneration. (D) Relative quantification (RQ)

by RTqPCR of *cd68* mRNA, marker of macrophages, within mdx and PLX3397-treated mdx calluses (mdx/PLX) at day 7 (d7). Expression level was normalized to GAPDH mRNA. (E) Stereological quantification of TRAP+ cells within mdx and PLX3397-treated mdx calluses (mdx/PLX) after 7 days (d7) of bone regeneration (left). Relative quantification (RQ) by RTqPCR of *matrix metallopeptidase-9 (mmp9)* mRNA (right), marker of osteoclasts, within mdx and PLX3397-treated mdx calluses (mdx/PLX) at day 7 (d7). Expression level was normalized to GAPDH mRNA. Error bars represent ±SEM. Unpaired Student's t test, P values *$p<0.05$, ***$p<0.0005$ (n=5 or 6 per group, n=3 per group for gene expression). Scale bar: 1 mm, 100 μ (B).

Table 1

Primers

Gene/mRNA	Forward Primer	Reverse Primer	Amplicon Length	GenBank Accession
BGLAP (OC)	Undisclosed	Undisclosed	102 bp	NM_007541
CD68	Undisclosed	Undisclosed	67 bp	NM_009853
Col1a1	Undisclosed	Undisclosed	98 bp	NM_007742
Col2a1	Undisclosed	Undisclosed	60 bp	NM_001113515 NM_031163
Col10a1	Undisclosed	Undisclosed	148 bp	NM_009925
MMP9	Undisclosed	Undisclosed	84 bp	NM_013599
VEGFa	Undisclosed	Undisclosed	117 bp	NM_001025250 NM_001110266 NM_001110267 NM_009505